Numerical investigations on the propagation of fire in a railway carriage.

CRAIG, M. and ASIM, T.

2020

energies

MDPI

Article

Numerical Investigations on the Propagation of Fire in a Railway Carriage

Matthew Craig and Taimoor Asim *

School of Engineering, Robert Gordon University, Aberdeen AB10 7GJ, UK; m.craig12@rgu.ac.uk

* Correspondence: t.asim@rgu.ac.uk

Received: 22 August 2020; Accepted: 22 September 2020; Published: 23 September 2020

Abstract: In this study, advanced Computational Fluid Dynamics (CFD)-based numerical simulations have been performed in order to analyse fire propagation in a standard railway compartment. A Fire Dynamics Simulator (FDS) has been employed to mimic real world scenarios associated with fire propagation within railway carriages in order to develop safety guidelines for railway passengers. Comprehensive parametric investigations on the effects of ignition location, intensity and cabin upholstery have been carried out. It has been observed that a fire occurring near the exits of the carriage results in a lower smoke layer height, due to the local carriage geometry, than an identical fire igniting at the center of the carriage. This in turn causes the smoke density along the aisleway to vary by around 30%. Reducing the ignition energy by half has been found to restrict combustion, thus reducing smoke density and carbon exhaust gases, reducing the average temperature from 170 °C to 110 °C. Changing the material lining of the seating has been found to cause the most significant change in output parameters, despite its relative insignificance in bulk mass. A polyester sample produces a peak carbon monoxide concentration of 7500 ppm, which is 27× greater compared with nylon. This difference has been found to be due to the fire spread and propagation between fuels, signifying the polyester's unsuitability for use in railway carriages.

Keywords: fire dynamics; Computational Fluid Dynamics (CFD); combustion analysis; smoke distribution; thermal plume

1. Introduction

Railway usage within the UK has steadily increased within the last five years, transporting on average around 440 million passengers in each yearly quarter [1]. Railway operators seek continuous improvement in both passenger comfort and safety, but ultimately also need palatable profit margins to sustain their business. Current technology now allows electric locomotives to run at a greater efficiency than diesel counterparts [2], and thus the electrification of the railway grid is commonplace across many EU member nations. Currently, 80% of current passenger kilometers are on electrified lines within the European region. Statistics show that railway travel produces 64% less CO_2 per passenger kilometer compared to automobiles [3,4]. Thus, the environmental and economic impacts of railway travel will further promote rail transport usage, highlighting the significance of understanding all aspects relevant to passenger safety.

Previous studies within the field of railway carriage safety highlight the criticality of fire eruption within an enclosed compartment [5–8]. Numerous investigations have been carried out to analyse the effects of ignition-related parameters, such as ignition position, ignition energy and combustive fuel, on the propagation of fire. This becomes increasingly important when fire ignition occurs whilst the train is in transit, essentially rendering escape impossible until the train comes to a stop. Thus, this study seeks to simulate propagation within the first 180 s after ignition, mimicking the suitable stopping time of a high-speed train and resulting escape period; a factor which is missing

in previous literature. A catastrophic event was the 2003 Daegu subway fire, wherein 148 people were killed. From the investigations, it was found out that the fire had taken only 2 min to engulf all six carriages [9]. Another example within the transport industry is Air Canada flight 797, where 23 passengers died due to a flash fire which started within the aircraft's toilet. Although the aircraft was on the ground when the fire was developing, many passengers were unable to evacuate the aircraft due to smoke intoxication [10]. Although the later event occurred within an aircraft, both cases share similarity in their occurrence within a compact space full of combustible materials. The rapid spread of fire within enclosed spaces highlights the necessity of an in-depth analysis into the fire dynamics and associated smoke generation and accumulation. In this study, we analyse fire propagation within a standard railway carriage, focusing on the first 180 s after ignition, based on the suitable stopping time of a high-speed train and passengers' escape period; a factor which is missing in most of published literatures. Furthermore, this study presents analysis on the effects of cabin upholstery, more specifically the material lining of the seating, on fire propagation. Previous works are severely limited in highlighting the extent of this parameter, and fail to investigate how relatively minor changes in bulk mass affect the propagation of fire. Thus, in the present study, extensive parametric analyses have been carried out using numerical investigations on the factors associated with fire propagation within railway carriages.

2. Literature Review

The enclosed nature and combustibility of a modern railway carriage emphasises the potentially catastrophic scenario of fire ignition. To remediate this effect, two of the standards which regulate material selection and standards specific to carriage design and maintenance are EN 50553—Requirements for running capability in case of fire on board of rolling stock and EN 45545—Railway applications: Fire protection on rolling stock [11]. These standards contain comparative information regarding oxygen index, flue gas density and smoke toxicity of materials and components, providing engineers with an analytical method of material selection within the railway industry [12].

The initial determinant of the severity of flame propagation is the ignition energy. The ignition heat release rate is the earliest indicator of potential intensity and thus suppression probability. Small scale testing conducted on seating taken from a decommissioned railway carriage [13] showed that higher magnitudes of ignition energy lead to rapid fire propagation and subsequent concentration of exhaust gases. The total time to complete combustion was 35% quicker when the ignition energy was doubled, indicating that the flame intensity and combustion rate are heightened under a larger heat energy source. The specific analysis of a compartmental fire conducted by Li et al. [14] found that when a fire of 1.5MW was under no forced ambient wind, only heights ≥70 cm above the ignition position caused a significant variation in temperature during the 800 s duration experiment. This was due to the thermal buoyancy of the smoke forcing the dispersion towards the 1 m high roof of the room. It must be noted, however, that the fire was fueled by Liquified Petroleum Gas (LPG) burner only, which would explain the relative lack of smoke density. Jia, Galea and Patel [15] discussed the differences between flame spread within enclosed and open compartments. It was found that fire within an enclosed setting initially produces rapid growth in both temperature and flame spread, compared with the open compartment, however it decays quicker due to oxygen deprivation. This does not necessarily reduce the thermal degradation of materials within the compartment, as the hot gas mixture present has enough energy to allow the endothermic pyrolysis to continue. An investigation into the 1985 British Airtours fight 28M using modern Computational Fluid Dyanmics (CFD)-based analysis concluded that a delay of 50 s in fire propagation could have saved all 55 lives lost in the disaster [16]. This further emphasises the destructive nature of fire within a compartment when considering that the ignition position was outside of the cabin, and local to the engine.

Characteristic fire progression within a compartment occurs within three phases: growth stage, stable stage and decay stage [17]. Typically, the growth stage contributes a sharp incline in total heat released, whilst the decay stage shows a reduction in heat release, albeit with a shallower gradient. Variations in the properties of fuel drive the fire progression, and thus the specific shape of the heat release curve. Research focusing on fire spread within an enclosed subway station showed both

carbon monoxide (CO) and carbon dioxide (CO_2) concentrations peaked between the third and fourth minute at a sensor located at the closest staircase to the point of ignition. Furthermore, the study showed that smoke flow velocity averaged between 0.5 and 1 m/s in the horizontal direction, and 3–5 m/s in the vertical direction across the 10-minute simulation time [18]. Molar concentrations of CO_2 were shown to be greatest at the flames, peaking at 0.015 kmole/m^3 during a methane fire within an enclosed compartment. In the same study, results showed that the concentration profile along the length of the compartment was mainly symmetrical, although it must be noted that the study focused on a burner with no further obstructions or combustible material to manipulate flame progression [19].

Smoke dispersion is dictated by two mechanisms: thermal plume and gravitational current [20]. Thermal plume creates a buoyant lift force to act on the smoke particulate due to the temperature difference and thus density difference between the hot exhaust gases and the cooler, ambient air. This effect causes smoke to immediately rise towards the roof within an enclosed space, and to spread along this equivalent plane [21]. Gravitational current is dictated by the mass of the smoke particulate weighing the flow down, causing the denser portion to flow closer to the ground, as per Newton's second law. This effect, however, is not present during the early stages of combustion, as the buoyant force of the smoke far exceeds the opposition to motion caused by the initial smoke density [22]. Heat distribution is dictated by smoke flow movement [23] until flashover occurs, when considering a large volume of enclosed space. Due to this, it has been observed that heat is distributed uniformly throughout a carriage soon after ignition [24].

Fire's toxicity, and thus its dispersion, poses by far the biggest risk of severe human injury. The asphyxiants CO and hydrogen cyanide (HCN) carry a life expectancy limit of 30 min within concentrations of 5700 ppm and 165 ppm, respectively. These compounds are seen to be most critical when involved in a compartmental fire, as there is greater chance of oxygen deprivation, causing the yields of these gasses to become more prominent [25,26]. When assessing historical cases of fire disaster, CO is the more prominent compound found within the bloodstreams of both injured and critically injured victims. In fact, it was found that, although given the lethality of HCN, the dosage with HCN was only a mere accessory to death in the presence of CO [27]. Nausea and disorientation occur in humans when carbon monoxide concentration levels exceed 70 ppm [28]. Likewise, carbon dioxide hinders judgement at levels of 3000 ppm [29]. It must be noted, however, that these figures are based on sole consumption and do not represent the true picture when there are many gases at play. The introduction of polymers as a fuel enhances the production of these (and others) gases. The constant evolution of material science has created an increasing number of individual variants of polymers, all with varying chemical and combustive properties, creating further issues in quantifiying the extent of their effects on humans. As with the applications of these materials, there tends to be many layers in their construction (such as adhesives), and it therefore becomes difficult to quantify which species of material is responsible for each specific reaction and to what extent [30]. A study emphasising these differences in the flammability of polymers showed significant fluctuations in the total heat released when the specifics of each individual polymer were varied. Using equivalent ignition heat across all samples, the total heat released differed by a multiple of four, and the time for sustained burn varied between 35 and 75 s [31].

The synthetic polymer Polyurethane Foam (PUF) is the most widely used material for commercial travel seating [32]. Although PUF takes a significantly longer time to fully combust compared with alternative natural materials such as horsehair or cotton, it produces considerably more lethal exhaust gases [33]. Through the combustion testing of a PUF sample, the exhaust density of carbon monoxide was found to be 2.32 mg/m^3, which resulted in a carbon-to-oxygen ratio of 15.26 [34]. In light of the above discussions, the aim of the preset study is to analyse the propagation of fire within a conventional railway carriage, with a view to understanding the complex dynamics of smoke generation and accumulation. For this purpose, numerical modelling techniques have been employed in the present study, the details of which are discussed in the next section.

3. Materials and Methods

Numerical modelling of the railway compartment has been carried out using an open source CFD code called Fire Dynamics Simulator (FDS) specifically designed to numerically analyse the dynamics of fire. This allows accurate smoke- and heat-driven flow illustrations to be visualised on FDS's sister program Smokeview. The main advantage of FDS is that it uses Large Eddy Simulation (LES) to resolve large eddies present in the flow, whilst modelling smaller ones. The time-based solution, with appropriate Courant number specifications, leads to a much higher accuracy in predicting the complex flow phenomena associated with fire dynamics, as compared to standard Reynolds-averaged Navier–Stokes (RANS)-based simulations.

3.1. Railway Carriage Model

Depicted in Figure 1a, the Siemens Viaggio Comfort is an example of an efficient (both environmentally and mechanically) model of train which is likely to replace diesel locomotives within Europe. The dimensions of the computational fluid domain are 26.5 m × 2.825 m × 2.8 m. Within this model, 84 seats are spaced evenly throughout the length of the carriage, with 4 seats per row either side of an aisleway, as shown in Figure 1b.

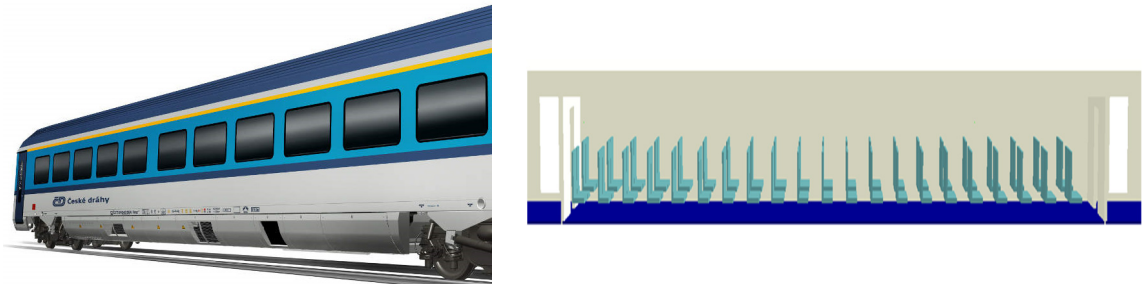

(**a**) (**b**)

Figure 1. (**a**) Siemens Viaggio Comfort [35]. (**b**) Side view of modelled carriage as modelled in Smokeview..

The specific geometries coded within FDS are illustrated within Table 1. It is worth noting here that the carriage walls have been considered to be adiabatic in the present study.

Table 1. Model's dimensional characteristics.

Characteristic	Dimension
Carriage length	26.5 m
Carriage width	2.825 m
Carriage height	2.8 m
Cabin length	21.5 m
Cabin partition wall thickness	0.4 m
Aisle width	0.9 m
Cabin door width	0.7 m
Cabin door height	1.985 m
Seating base	0.45 × 0.4 × 0.1 m
Seating back	0.06 × 0.4 × 0.85 m
Leg room (base to back)	0.541 m
Number of seating rows	21
Number of seats	84

3.2. Spatial Discretisation of the Railway Carriage

Spatial discretisation is the process of dividing the model into parts, so that the flow governing equations can be solved in each part. This division process is known as meshing, completed by

specifying face sizes in each directional plane, allowing the number of elements or sub-volumes to be calculated. Due to the large size of a railway carriage, computational power must be used in accordance with mesh sensitivity to effectively model this scenario. To allow multiple computational processes to occur simultaneously, the carriage was split into three sections in the x-direction, producing three meshes which were identical in size of elements. The face size used within this model is 12 cm across all three meshes. Mesh independence studies carried out (in Section 3.1) depict that a 12 cm mesh sizing is most appropriate for carrying out the fire dynamics analysis in the given conditions.

3.3. Fire Propagation Governing Equations

Three dimensional Navier–Stokes equations, along with the mass conservation equation, have been iteratively solved for the turbulent and transient flow within the railway carriage. Equation (1) controls the time step throughout the simulation, according to Courant, Friedrichs and Lewy (CFL) conditions [36]:

$$\Delta t = \frac{5 \cdot \sqrt[3]{\delta x \delta y \delta z}}{\sqrt{g \cdot H}} \quad (1)$$

Combustion models are calculated in each time step. Flow turbulence is modelled using the Large Eddy Simulation (LES) model. This allows an accurate representation of the flow turbulence by resolving for large-scale eddies, whilst modelling smaller-scale eddies in the flow. For modelling small-scale eddies, a sub-grid scale (SGS) has been employed [37,38], which is specified by an algebraic relationship based on scale similarity [39]. The filter width has been defined by the cubic root per cell volume. When corresponding to continuous fields, the filtered field is as expressed in Equation (2).

$$\overline{\emptyset}(x, y, z, t) \equiv \frac{1}{\delta x \cdot \delta y \cdot \delta z} \int_{x-\frac{\delta x}{2}}^{x+\frac{\delta x}{2}} \int_{y-\frac{\delta y}{2}}^{y+\frac{\delta y}{2}} \int_{z-\frac{\delta z}{2}}^{z+\frac{\delta z}{2}} \overline{\emptyset}(x', y', z', t) dx' dy' dz' \quad (2)$$

Definition of the SGS stress is required in order to correlate the Favre filtered velocity vectors. This is expressed in Equation (3).

$$\tau_{ij}^{sgs} \equiv \overline{\rho}\left(\widetilde{u_i u_j} - \tilde{u}_i \tilde{u}_j\right) \quad (3)$$

To render the equation in FDS, the total deviatoric stress must be known. This expression is shown in Equation (4).

$$\tau_{ij}^{dev} \equiv \overline{\tau}_{ij} + \tau_{ij}^{sgs} - \frac{1}{3}\tau_{kk}^{sgs}\delta_{ij} = -2(\mu + \mu_t)\left(\tilde{S}_{ij} - \frac{1}{3}(\nabla \cdot \tilde{u})\delta_{ij}\right) \quad (4)$$

The isotropic component of SGS stress must be absorbed by the pressure term. This is done by first defining the sub-grid kinetic energy and therefore defining the filtered pressure term, illustrated in Equation (5).

$$\bar{p} \equiv \overline{p} + \frac{2}{3}k_{sgs} : k_{sgs} \equiv \frac{1}{2}\tau_{kk}^{sgs} \quad (5)$$

Equations (4) and (5) are then combined with the momentum equation, as shown in Equation (6).

$$\frac{\partial \overline{\rho}\widetilde{u_i}}{\partial t} + \frac{\partial}{\partial x_j}(\overline{\rho}\tilde{u}_i\tilde{u}_i) = -\frac{\partial \overline{\rho}}{\partial x_i} - \frac{\partial \tau_{ij}^{dev}}{\partial x_j} + \overline{\rho}g_i + \bar{f}_{d,i} + \overline{\dot{m}_b'''}\tilde{u}_{b,i} \quad (6)$$

3.4. Material Properties

To understand the effects of material selection on the propagation and growth of fire, two alternative seat linings have been identified. As previously discussed, polyurethane foam is considered the most popular choice of foam for cushioning in commercial and home furniture, and thus has been chosen as a baseline material within both models. A Polyamide/Nylon 6 (PN6)-type sample has been chosen as a potential material for the fabric lining of seating due to its high ductility and relatively low

combustion rate [40]. To coincide with this, a Polyester fabric (PLY)-type lining has also been used for comparison purposes, as this material has superior fatigue and workability properties. Previous work carried out by Węgrzyński and Vigne [41] emphasises the importance of pre-defined soot yield in the visibility, and thus density, in smoke production. Through past experimentation, the values of soot and carbon monoxide yields were defined by the Society of Fire Protection Engineers (SFPE), table A.39 [42]. Further details of the selected materials have been summarised in Table 2.

Table 2. Properties of materials selected.

Characteristic	Polyurethane Foam	Nylon	Polyester
Molecular formula	C2.5	C1.2	C1.0
	H4.2	H2.2	H0.8
	N0.2	N0.2	N0.1
	O0.6	O0.2	O0.4
Density (kg/m³)	17.00	1130.00	1380.00
Specific heat capacity (J/kg·K)	1.45	1.90	1.20
Thermal conductivity (W/m·K)	0.26	0.15	0.50
Heat of reaction (kJ/kg)	710	820	795
Heat of combustion (kJ/kg)	25300	23633	23800
Soot yield (g/g)	0.131	0.075	0.080
CO yield (g/g)	0.010	0.038	0.089
Seating colour (Solely illustrative)	-	Teal	Red

To confirm gas species after the multi-phase reaction, the components of each element have been calculated using the stochiometric balancing equation. Due to limitations in using FDS, nitrogen is balanced to N_2. This is shown in Equation (7)

$$C_X H_Y O_Z N_\nu + \nu_{O_2} O_2 \xrightarrow{\text{yields}} \nu_{CO_2} CO_2 + \nu_{H_2O} H_2O + \nu_{CO} CO + \nu_S Soot + \nu_{N_2} N_2 \quad (7)$$

The molar mass of the fuel was calculated using Equation (8), as below. As FDS assumes soot to be composed of carbon and hydrogen [43], the molecular mass of soot is reduced to Equation (9).

$$m_F = x \cdot m_C + y \cdot m_H + z \cdot m_O + v \cdot m_N \quad (8)$$

$$m_S = X_H \cdot m_H + (1 - X_H) \cdot m_C \quad (9)$$

Thus, the stochiometric coefficients for CO and soot are calculated using Equation (10).

$$\nu_{CO} = \frac{m_F}{m_{CO}} \cdot Y_{CO} : \ \nu_s = \frac{m_F}{m_s} \cdot Y_s \quad (10)$$

In order to calculate the unknown coefficients, the known atomic balances are arranged in matrix form, as shown in Equation (11).

$$\begin{bmatrix} 1 & 0 & 0 & 0 \\ 0 & 2 & 0 & 0 \\ 2 & 1 & 0 & -2 \\ 0 & 0 & 2 & 0 \end{bmatrix} \begin{Bmatrix} \nu_{CO_2} \\ \nu_{H_2O} \\ \nu_{N_2} \\ \nu_{O_2} \end{Bmatrix} = \begin{Bmatrix} x - \nu_{CO} - \nu_s(1 - X_H) \\ \nu_{H_2O} \\ \nu_{N_2} \\ \nu_{O_2} \end{Bmatrix} \quad (11)$$

The corresponding products of each species' reaction are illustrated in Table 3.

Table 3. Stoichiometric coefficients of materials in reaction phase.

Stochiometric Coefficients	Products PUF	Products PN6	Products PLY
ν_{CO_2}	1.979113	1.029281	0.789749
ν_{H_2O}	0.384504	2.071987	0.391591
ν_{CO}	0.044164	0.016659	0.058886
ν_s	0.309912	0.560253	0.168184
ν_{N_2}	0.100000	0.100000	0.050000
ν_{O_2}	2.723436	1.490774	0.814987

3.5. Boundary Conditions

In order to evaluate the effects of ignition on fire propagation within the railway carriage, two different ignition points have been selected; one in the centre of the carriage (R11, S3) and one near the front (R1, S1). Air-conditioning units have been spaced evenly along either side of the aisle. Visual placement of these boundary conditions are depicted in Figure 2.The Air-conditioning (AC) units are set to operate at an airspeed of 0.1 m/s, defined as the maximum mean air velocity within ISO 7730: Ergonomics of the thermal environment [44].

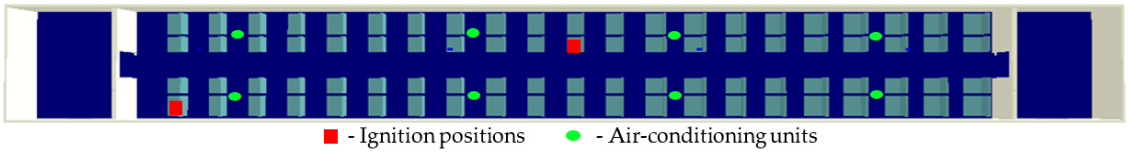

Figure 2. Ignition and air-conditioning within the railway carriage.

In order to specify the ignition heat release rate to a multi-phase reaction, the mass flux has been calculated for each material for each ignition rate considered in the present study. A constant, β, is added to regulate the mass split between the foam and the lining. Within the calculations, the mass of foam has been specified as 98% of the overall mass flux split, therefore concluding that the seat lining comprised 2% of the mass split. This is shown in Equation (12) with the calculated results of each mass flux per each ignition heat release rate. The resultant parameters have been summarised in Table 4.

$$j_m = \frac{\beta \cdot \dot{q}_{ign}}{A_{ign}} \cdot \frac{1}{\Delta H_c} \quad (12)$$

Table 4. Proportional mass flux split per material.

Material	Ignition Heat Release Rate (kW)	Mass Flux of Foam (g/m²·s)	Mass Flux of Lining (g/m²·s)
PN6	250	53.7989	1.1754
	125	26.8994	0.5877
PLY	250	53.7989	1.1671
	125	26.8994	0.5836

In order to record data for smoke density, chemical concentration and temperature, 5 sensors have been evenly spaced within the railway carriage, ascending along the central axis of the aisle at a height of 1.7 m (average height of passengers). Given the scenario assessed and the fact that CO output is dependent on incomplete combustion, the data recorders have been set to monitor levels of CO and CO_2 only throughout the simulation time. In order to fully analyse the effects of fire at the point of highest endangerment, the carriage has been considered to be fully enclosed, so as to model a fire when the carriage is in transit.

4. Results and Discussion

4.1. Mesh Independence Testing

In order to verify the numerical predictions, a detailed and systematic mesh independence study was carried out. A primary face size of 15 cm was reduced by 10% incrementally until the results obtained were independent of the mesh size. As smoke density forms the basis of the present study, it was considered as the primary parameter for mesh independence testing. The average smoke density reading across the length of the railway carriage with respect to time from ignition is shown in Figure 3, for the different mesh sizes considered. Given the dependency on computational power that CFD demands, especially in the case of energy transport, the criteria of convergence was a ≤15%

difference in readings between respective meshes. It can be clearly seen that mesh sizes of 12 cm, 13.5 cm and 15 cm all predict the smoke density with reasonable accuracy, and thus, a mesh size of 12 cm was chosen for conducting further analyses in the present study.

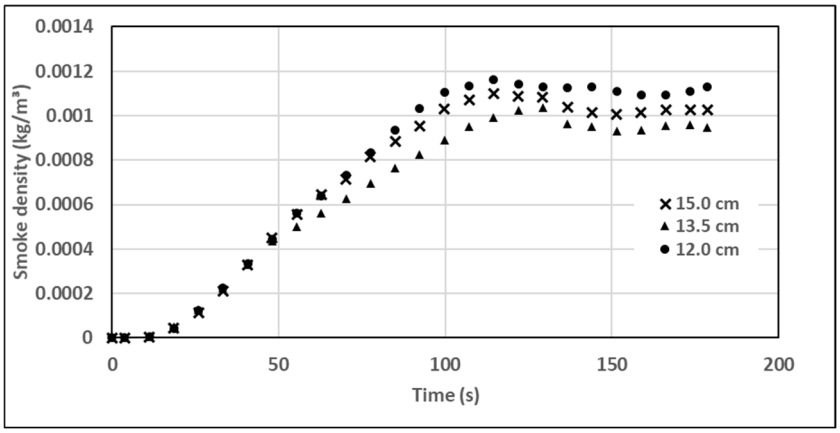

Figure 3. Mesh independence results.

4.2. Effects of Ignition Position

The ignition position was found to have a significant effect on the propagation of fire and smoke. As shown in Figure 4, the smoke dispersion varied considerably during the early stages of fire ignition and progression, but slowly became more uniform after 50 s of ignition. This is due to thermal buoyancy, which forces the hot smoke to travel upwards and thereafter along the length of the roof. Once the roof area has been encompassed in smoke, it begins to accumulate within the volume of the carriage due to gravitational current. It was noticed that after 100 s, the entire carriage was completely filled with smoke.

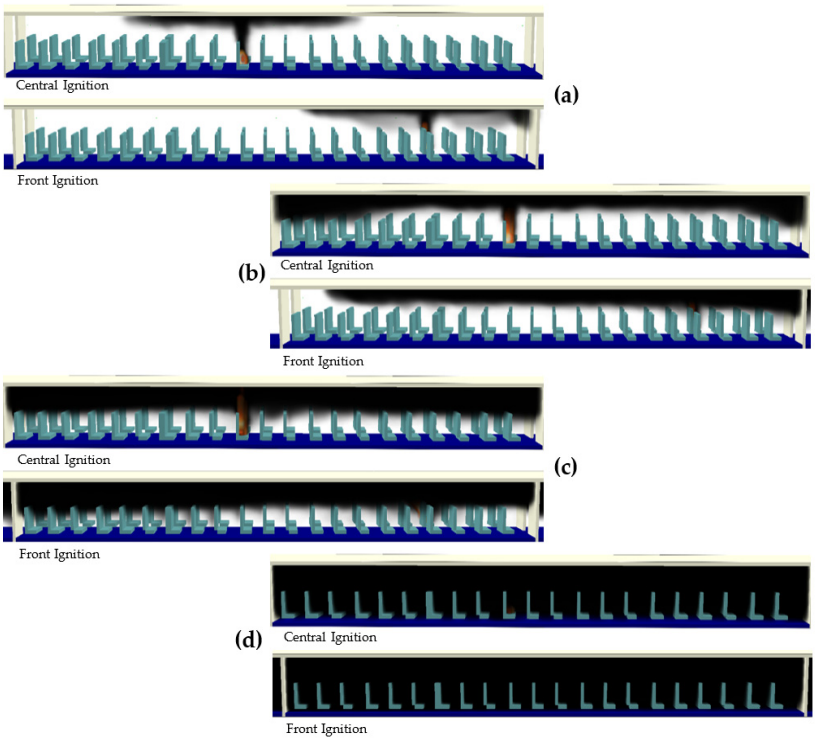

Figure 4. Smoke distribution due to varying ignition position after (**a**) 10 s; (**b**) 30 s; (**c**) 50 s; (**d**) 100 s.

By analysing the smoke distribution within the railway carriage quantitatively, for both the central and front ignition positions, it can be seen (in Figure 5a) that during the initial few seconds

after ignition, there were negligibly small fractions of smoke present in the carriage. Thus, the initial few seconds are most crucial for evacuation. Sensor 1, which was barely 1.5 m away from the front ignition position, then recorded a steep increase in smoke density, whilst the smoke reached the further sensors (sensors 3 and 5) after a few more seconds. As sensors 2 and 4 depicted the same trends as sensors 3 and 5, their recorded data has not been shown here. It can be further seen that in the case of central ignition, the smoke density continued throughout the carriage; however, the rate of increase in smoke density decreased with time as more of the carriage filled with smoke. Smoke propagation in the central ignition configuration continued up to 120 s, after which sensors 1 and 3 (furthest sensors in this scenario) showed a decrease in smoke density, whilst the closest sensor showed stable (almost constant) values. This is because of the air-conditioning system having a greater venting effect when the smoke becomes stagnant.

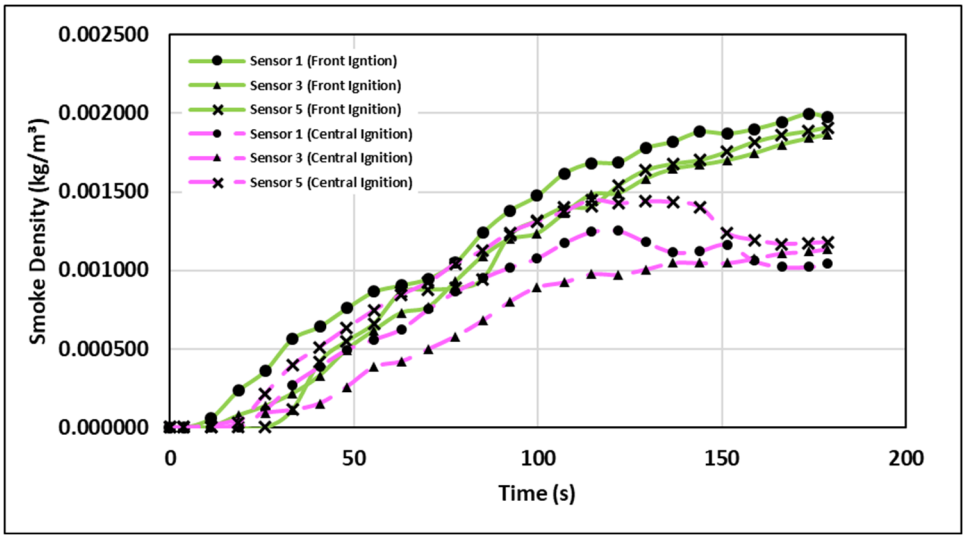

(**a**)

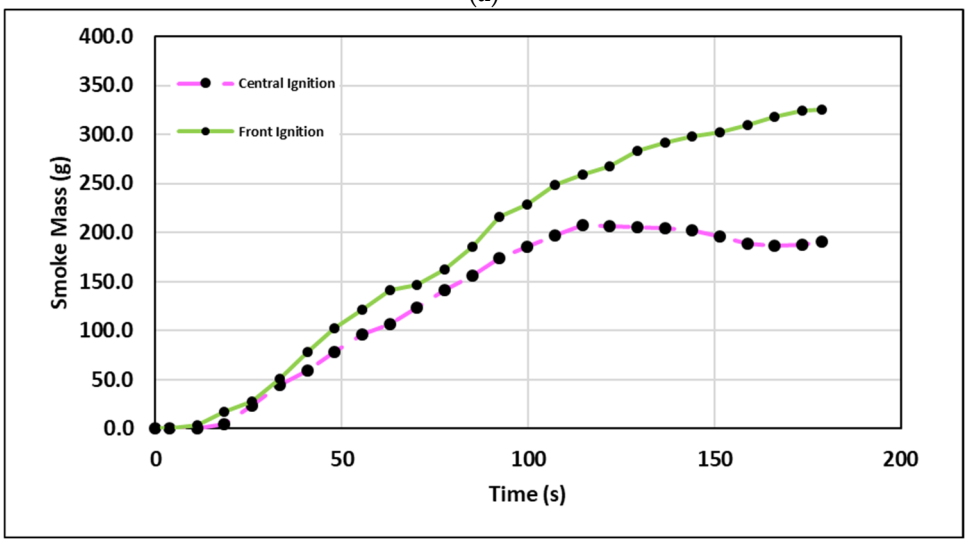

(**b**)

Figure 5. (**a**) Smoke density comparison for different ignition positions. (**b**) Smoke mass comparison for different ignition positions.

Smoke propagation in the central ignition configuration continued up to 120 s, after which sensors 1 and 3 (furthest sensors in this scenario) showed a decrease in smoke density, whilst the closest sensor showed stable (almost constant) values. This is because of the air-conditioning system having a greater venting effect when the smoke becomes stagnant. Overall, it can be seen that the smoke density within the central ignition was around 30% less than the front ignition. This is due to the

smoke layer height being lower within the front ignition, as the smoke can only travel in three directions rather than four (due to the partition wall), causing the smoke to travel downwards more quickly.

A comparison of the indictive mass of smoke present within the carriage is shown in Figure 5b. Mass was calculated using the average values across the five sensors for each time interval within the volume of the carriage. The trends show that the smoke mass for the central ignition model remained constant after 118 s. This suggests that either the fire fully burned out the mass which it was ignited on or the forces of gravitational current and thermal buoyancy were at different ratios in each model, causing the smoke layer height to be different at each time interval.

Figure 6, which depicts the temperature variations along the central axis of the carriage, clearly shows that gas temperature was significantly higher in the front ignition configuration. This is due to smoke dispersion across the carriage. Correspondingly, the temperature profiles depicted in Figure 7a follow similar trends in relative magnitude to the sensor-recorded values of smoke density. This implies that the temperatures measured are primarily dependent on the smoke. When comparing this to data recorded for carbon exhaust gases shown in Figure 7b, the notion that smoke toxicity is by far the greatest risk to human life within the early stages of fire is reinforced.

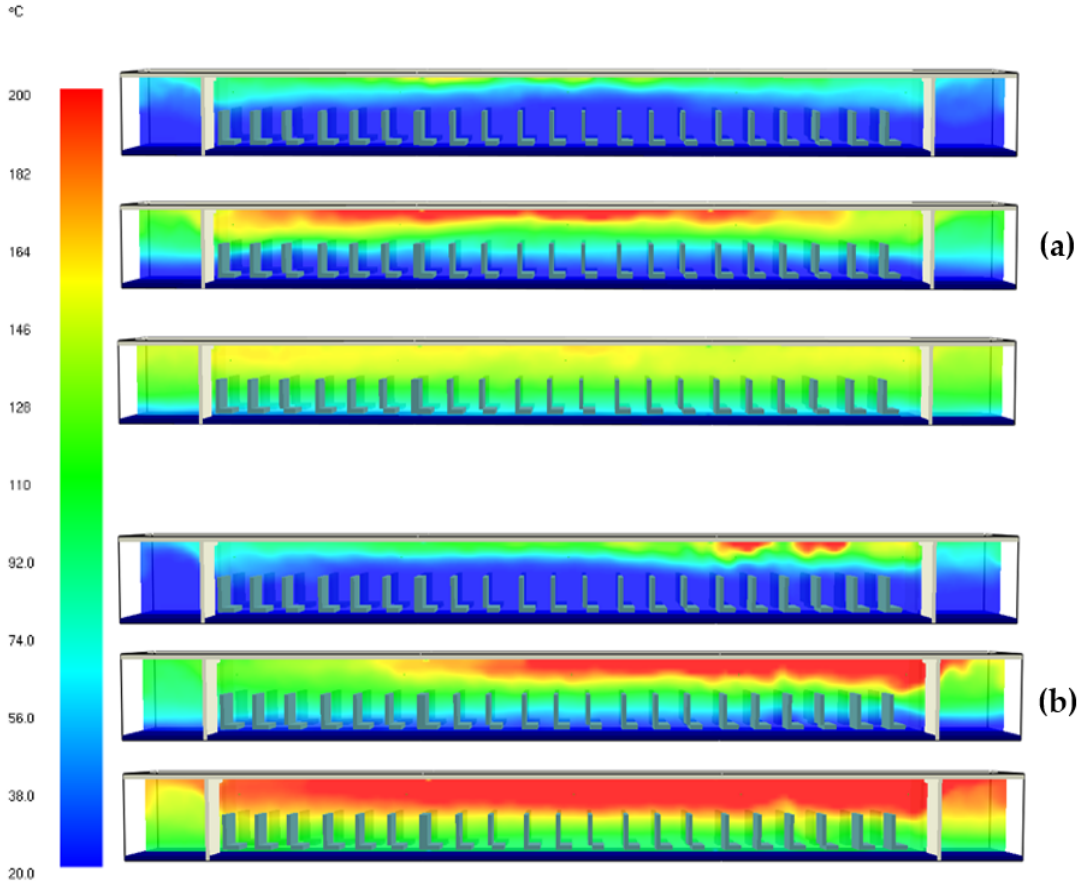

Figure 6. Gas temperature variations along the central plane of carriage after 40 s, 80 s and 120 s for (**a**) central ignition and (**b**) front ignition.

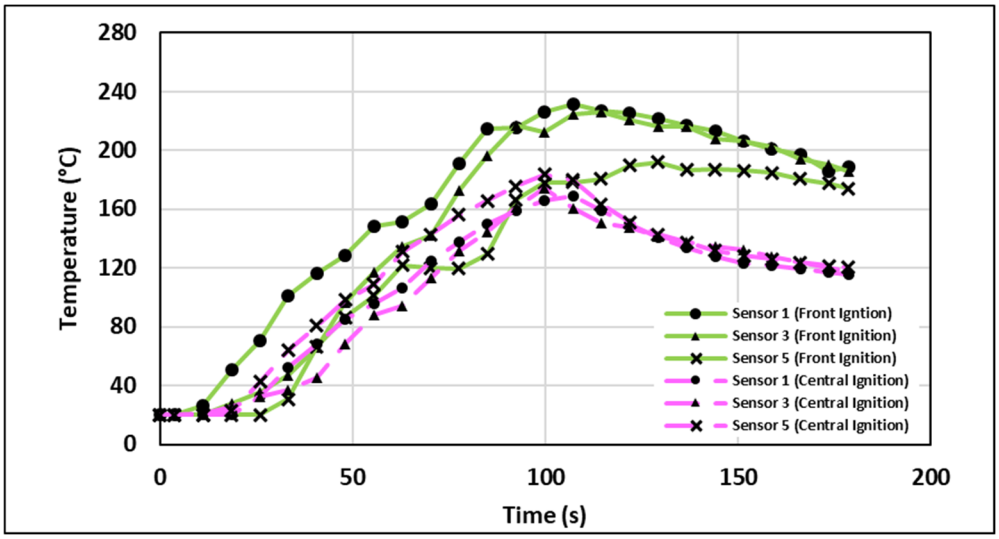

(**a**)

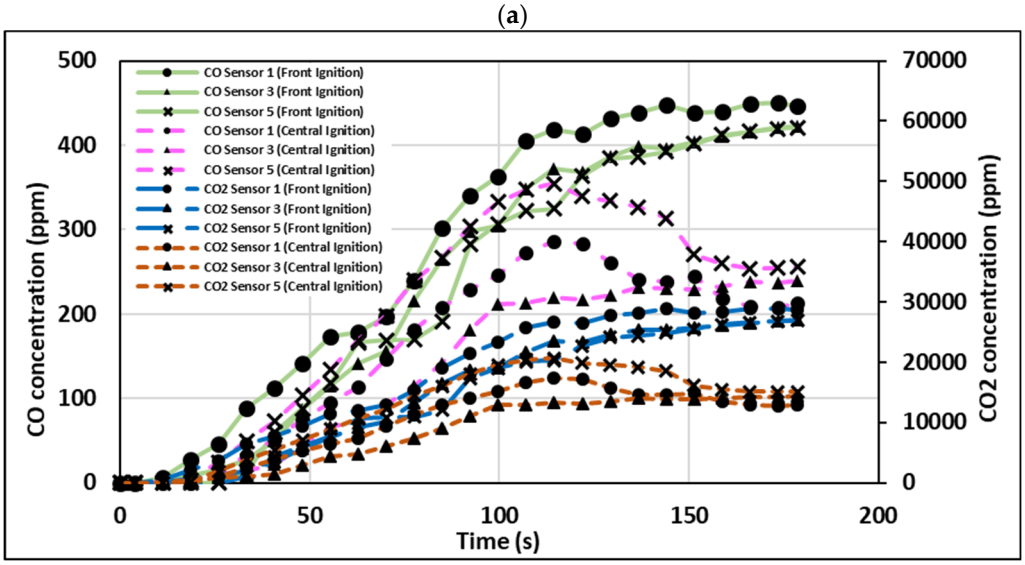

(**b**)

Figure 7. (**a**) Temperature profile comparison due to ignition position. (**b**) Carbon gases concentrations for different ignition positions.

It can be seen in both the models that concentrations of both of CO and CO_2 exceeded the dangerous levels of potential human incapacity (70 ppm and 3000 ppm respectively), 60 s after ignition, across all sensors. Although these levels are not sufficient to cause significant respiratory harm within the short term, hampered judgement within critical situations such as an evacuation would inevitably cause its own issues. There was also a noticeable difference in standard deviation across the sensors for each ignition position. The front ignition showed significantly greater initial dispersion between sensors 1 and 3, and sensor 5, when compared with the more uniform progression in the case of central ignition. This is due to the smoke taking more time to travel the entire length of the carriage to reach sensor 5, and the overall profile across the carriage thus being more varied.

4.3. Effects of Ignition Heat Energy

Historical fire scenarios within the railway industry have shown that ignition energy is suspect to change depending on the circumstances around the fire, such as an accelerant-based arson [45]. When reducing the initial ignition heat energy by half, the toxicity of smoke and temperature has been found to reduce. The smoke dispersion, shown in Figure 8, depicts that there is little difference in smoke propagation between the two ignition configurations, i.e., high ignition of 250 kW and low

ignition of 125 kW. The results suggest that the difference in ignition energy does not significantly influence the velocity of product gases under the given conditions.

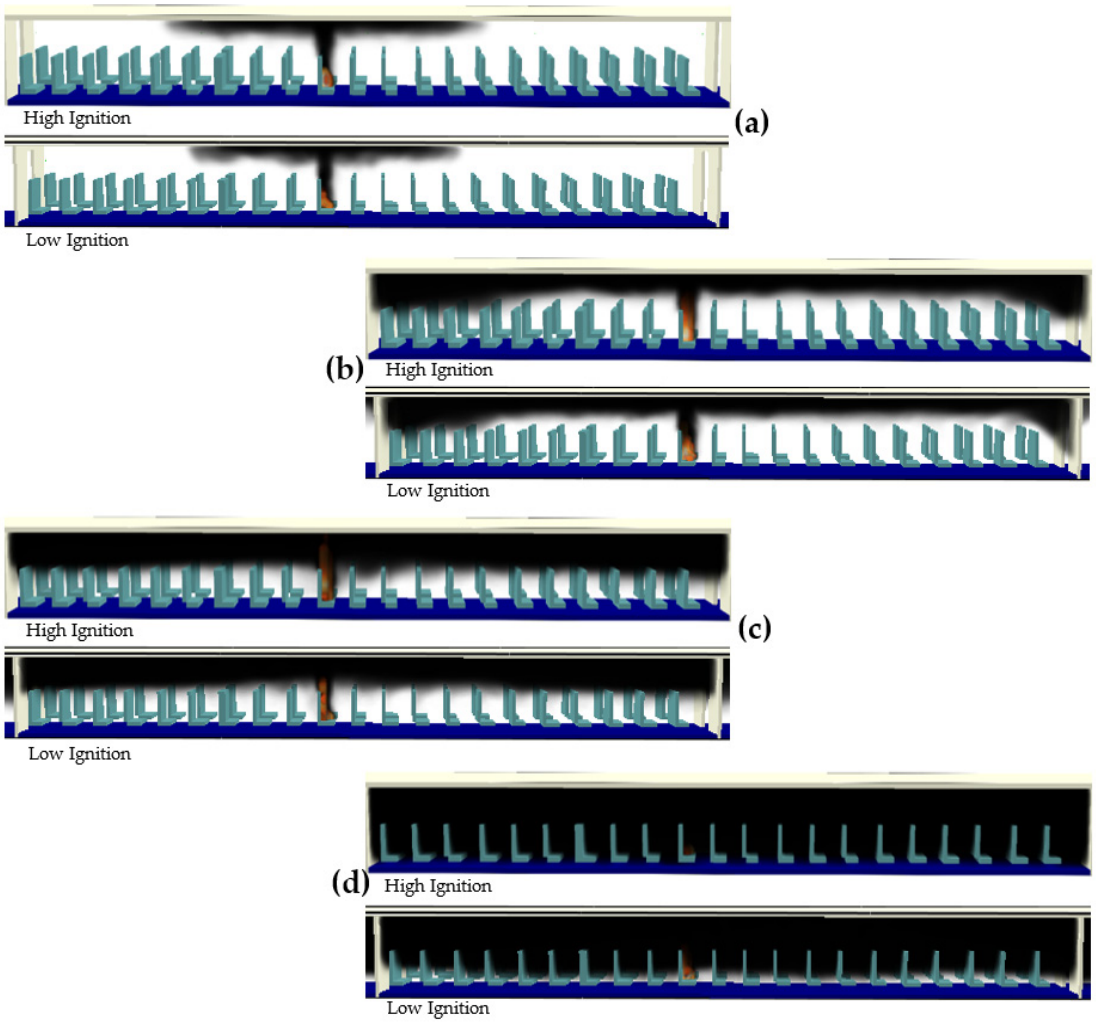

Figure 8. Smoke distribution due to varying ignition energy at (**a**) 10 s, (**b**) 30 s, (**c**) 50 s, (**d**) 100 s.

When analysing the comparison of smoke density measured, it is clear that although the smoke dispersion was visually similar, the higher ignition model had around a 16% greater average smoke mass compared to the lower ignition model, as shown in Figure 9a. This was to be expected as the higher the heat release rate, the higher will be the thermal energy conversion, and more gases will be produced. Furthermore, it can be seen that sensor 5 records the highest smoke density for both simulations at the same time instances. A comparison of the mass of smoke present within the carriage is shown in Figure 9b for the two ignition rate simulations. It can be seen that both ignition heat energies followed similar trends; however, the higher ignition model possessed around 14% more smoke mass than the lower ignition model. Furthermore, on analysing smoke production after 10 s, the ratio between the models fluctuated between 1.28 and 1.42, indicating that ignition energy is directly responsible for smoke production.

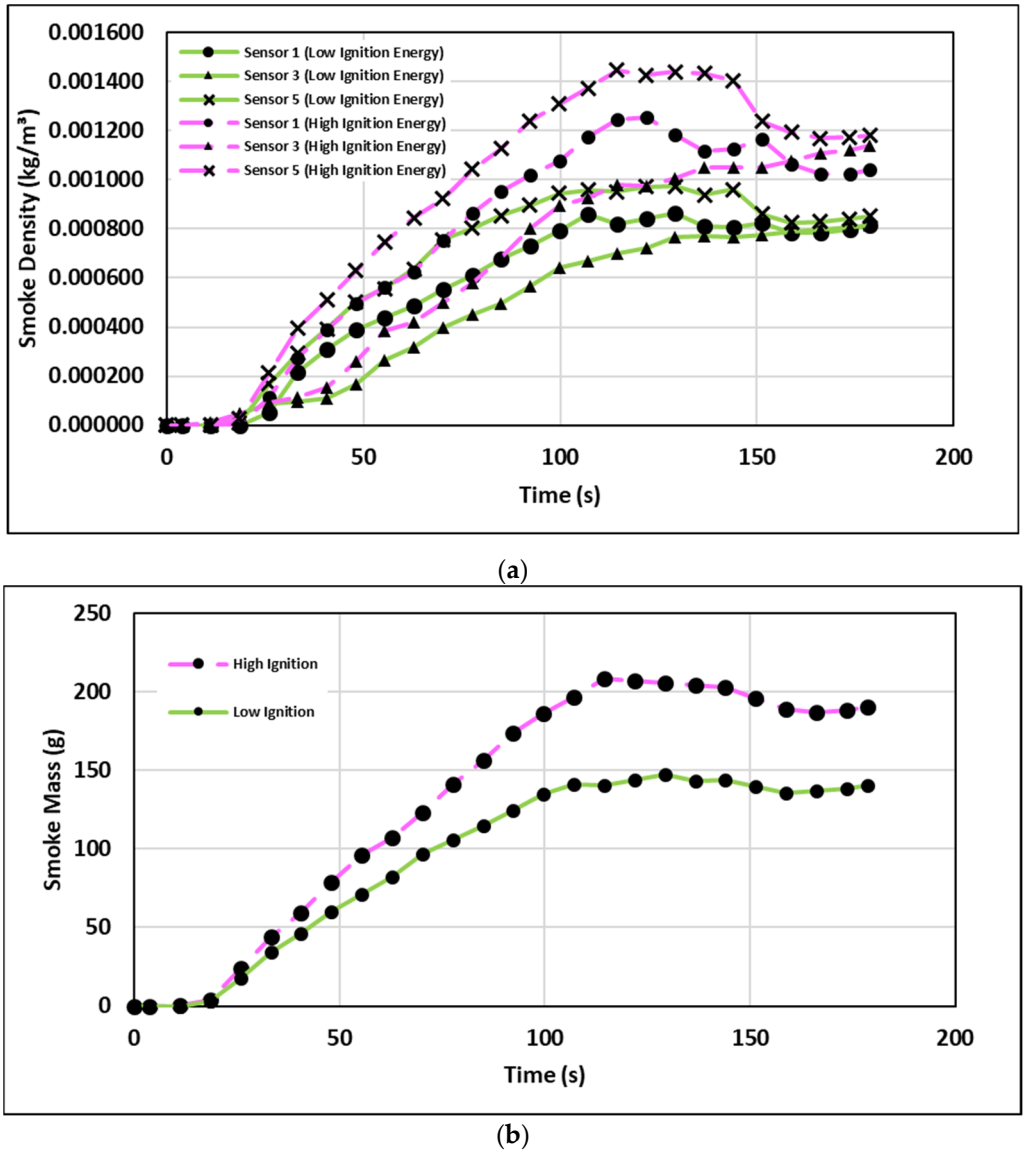

Figure 9. (**a**) Smoke density comparison due to varying ignition energy. (**b**) Smoke mass variations due to different ignition energy.

Figure 10 depicts the variations in temperature gradients along the central axis of the carriage between the low and high ignition modes. It can be clearly seen that similar patterns exist, however, the higher ignition energy represents a bigger range of temperatures, emphasising the greater heat across the cabin. Furthermore, the enhanced effect of gravitational current within the high ignition model is shown, as the greater spread of temperature in the y-direction gives a good indication of the reduced smoke layer height between the two models. Temperature data is quantified in Figure 11a, depicting how the temperature profiles progressed over time at each sensor for both the ignition modes. As expected, when analysing each individual sensor, it is seen that the model with the higher heat energy resulted in higher temperatures across the carriage. Both models showed similar growth trends, with the rate of change decreasing after 100 s, and with the high ignition model recording around 50 °C (or 40%) higher temperature readings. One recommendation to remediate the significant effect that initial ignition heat release has on the overall growth of fire is to increase the number of mobile fire extinguishers, and to have them equally spaced throughout the carriage. This would allow one to slow down fire propagation from an early stage and substantially decrease the potential hazards from it. Analysing the toxicity of smoke in the carriage, Figure 11b shows that

although the lower ignition energy corresponded to lower readings of both CO and CO_2 concentrations, these were not correspondingly half of those related to the higher ignition energy.

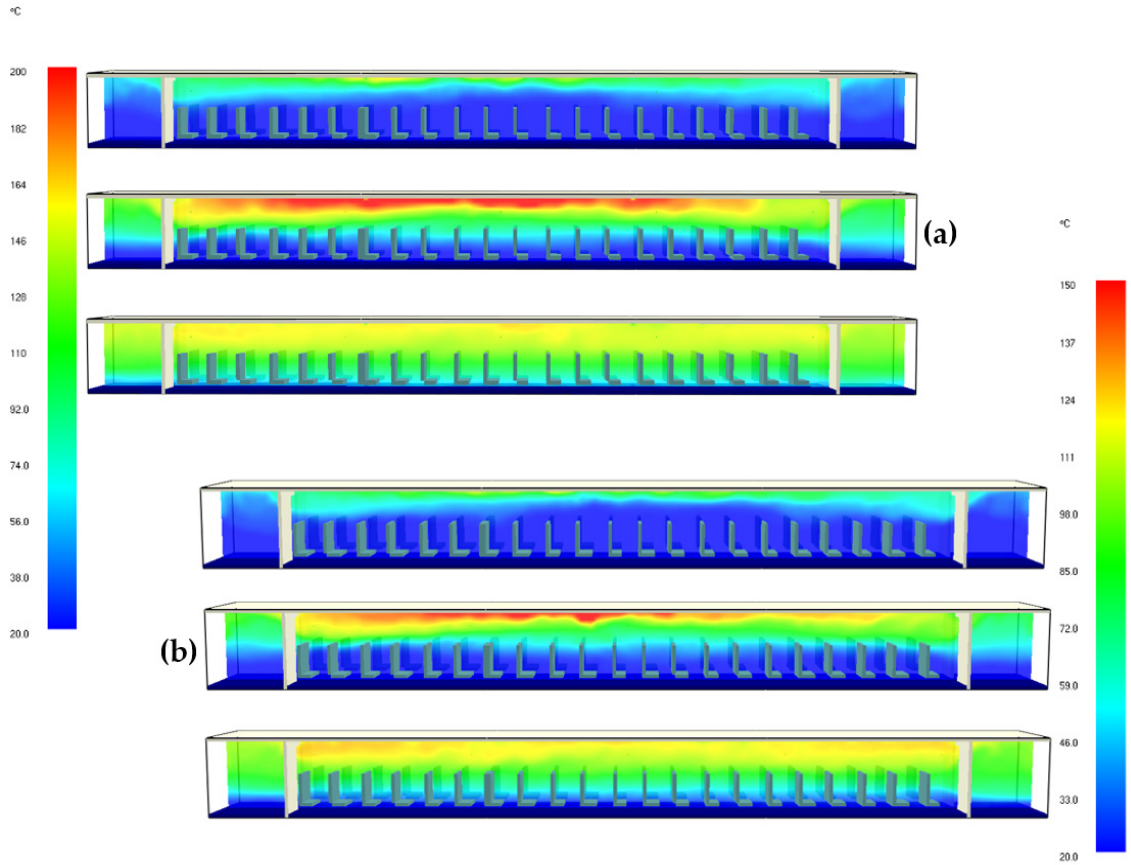

Figure 10. Temperature variations along the central plane of the carriage after 40 s, 80 s and 120 s for (**a**) high ignition model and (**b**) low ignition model.

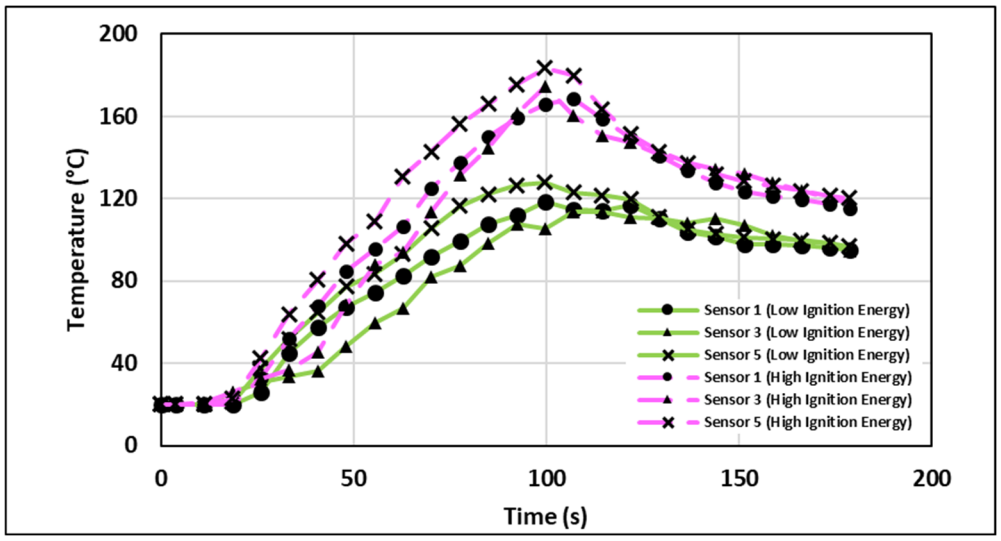

(**a**)

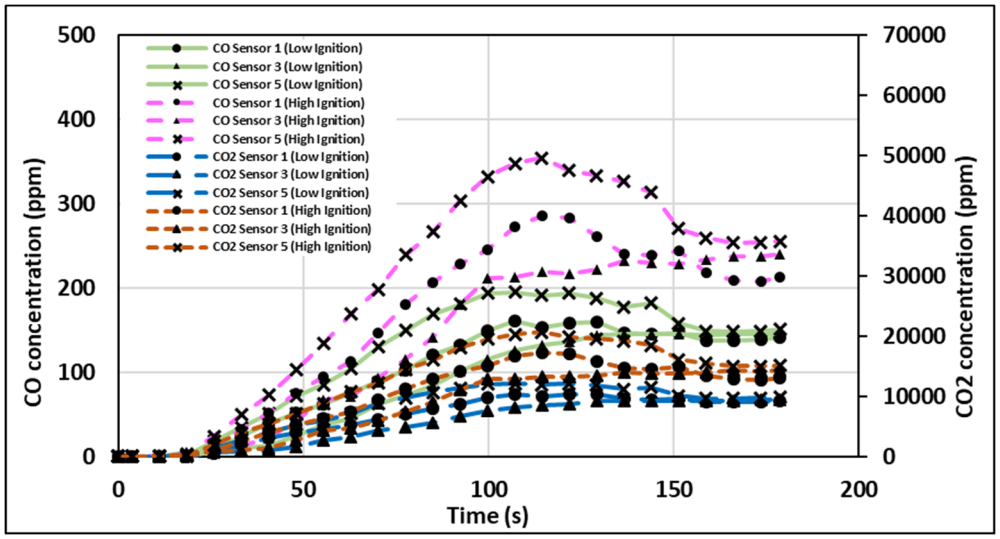

(**b**)

Figure 11. (**a**) Temperature variations due to ignition energy. (**b**) Carbon gases concentrations for different ignition energies.

Further analysis of the data in Figure 11b reveals that in the lower ignition energy model, the concentrations of both gases exceeded the potential incapacity levels after 80 s across all sensors. In the worst possible scenario of a fire igniting when the train is at high-speed, it is reasonable to assume the time between ignition and possible passenger escape to be around 90 s. The severity of the situation, even with the lower ignition model, emphasises the need to tackle the fire quickly—as close to the ignition as possible—in order to inherently slow down the propagation of fire.

4.4. Effects of Cabin Upholstery

Varying the seating material lining has been found to have a significant impact on the toxicity and propagation of fire within a railway carriage, despite its relatively low combustible mass. The smoke dispersion, shown in Figure 12, depicts that the generation and movement of smoke, along the length of the carriage, did not significantly vary between the NYL and PN6 materials along the x-direction. Smoke density data recorded for the PLY model, as shown in Figure 13a, depicts the similar growth between both material lining models within the 100 s after ignition. Within the following 40 s, however, the polyester-type lining saw considerable growth, recording values of soot density four times greater than the recorded data for the nylon-type model. The smoke flow movement versus the smoke density profile suggests that the PLY lining is more susceptible to fast combustion, giving the flames greater energy when combusting the polyurethane foam cushioning. This scale difference can also be seen in smoke mass, depicted in Figure 13b.

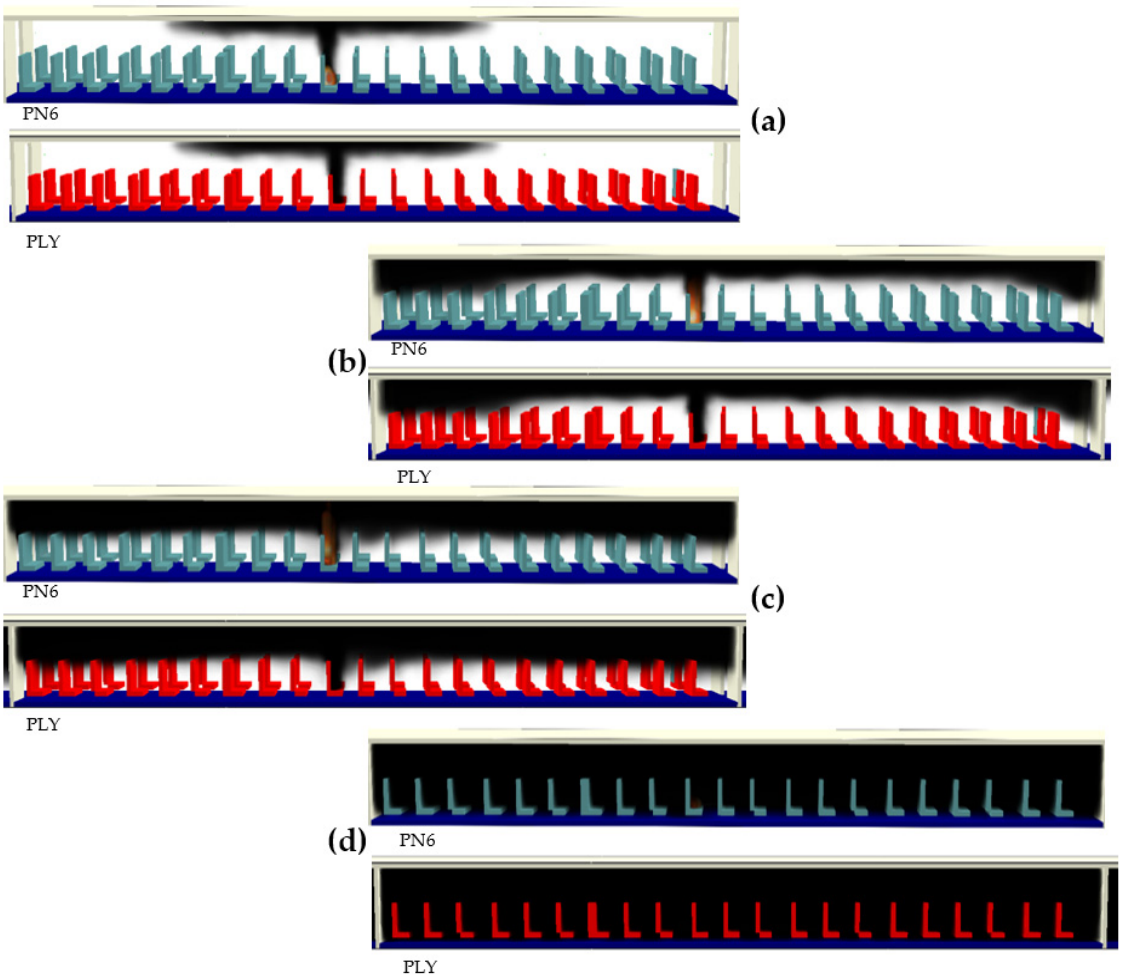

Figure 12. Smoke distribution for different seating materials after (**a**) 10 s, (**b**) 30 s, (**c**) 50 s, (**d**) 100 s.

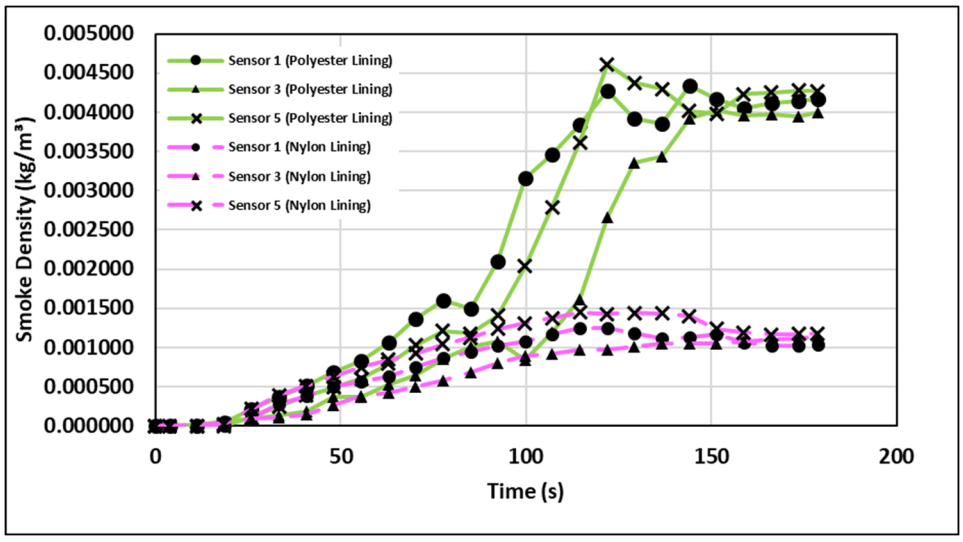

(**a**)

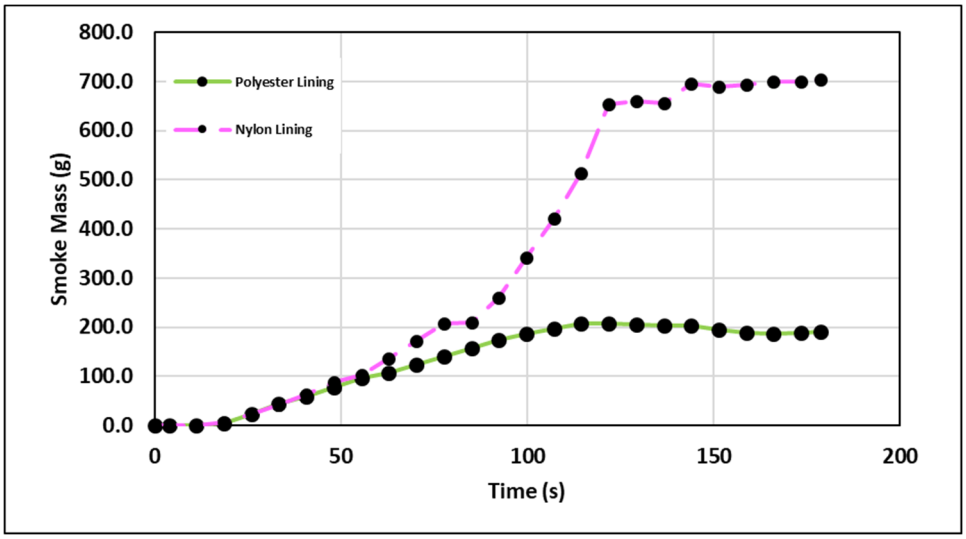

(**b**)

Figure 13. (**a**) Smoke density comparison for different seating materials. (**b**) Smoke mass variations for different seating materials.

The drastic increase in smoke density after 100 s would lead to the conclusion that the fire within the PLY seat lining spreads to the surrounding seating. This is validated in Figure 14, which depicts a snapshot of the flame spread within the polyester-type model 125 s after ignition. This flame spread therefore had a significant effect on the temperature profile across the compartment. As shown in Figure 15, both models had relatively similar temperature contours after 80 s. It was only after 120 s that the temperature within each compartment differed substantially, suggesting that the additional heat was primarily caused by the flame spread. This is in part validated in Figure 16a, which shows that sensor 3 (the closest sensor to the ignition point) had a maximum recorded value of almost double that of sensors 1 and 5 within that simulation. When considering historical fires within the railway industry, such as the Howard Street tunnel fire, temperatures have been recorded to have exceeded ≥1200 °C in places [46], which is in line with the results obtained in the present study. The flames themselves cannot be seen within Figure 15 due to the differing position of the ignition and contour plane.

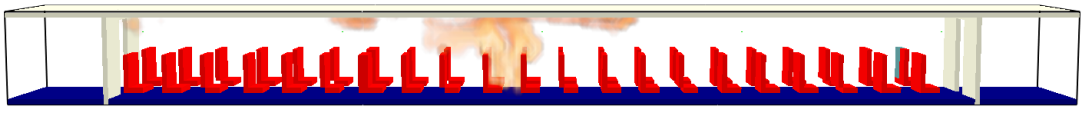

Figure 14. Flame spread within the polyester-type lining after 125 s.

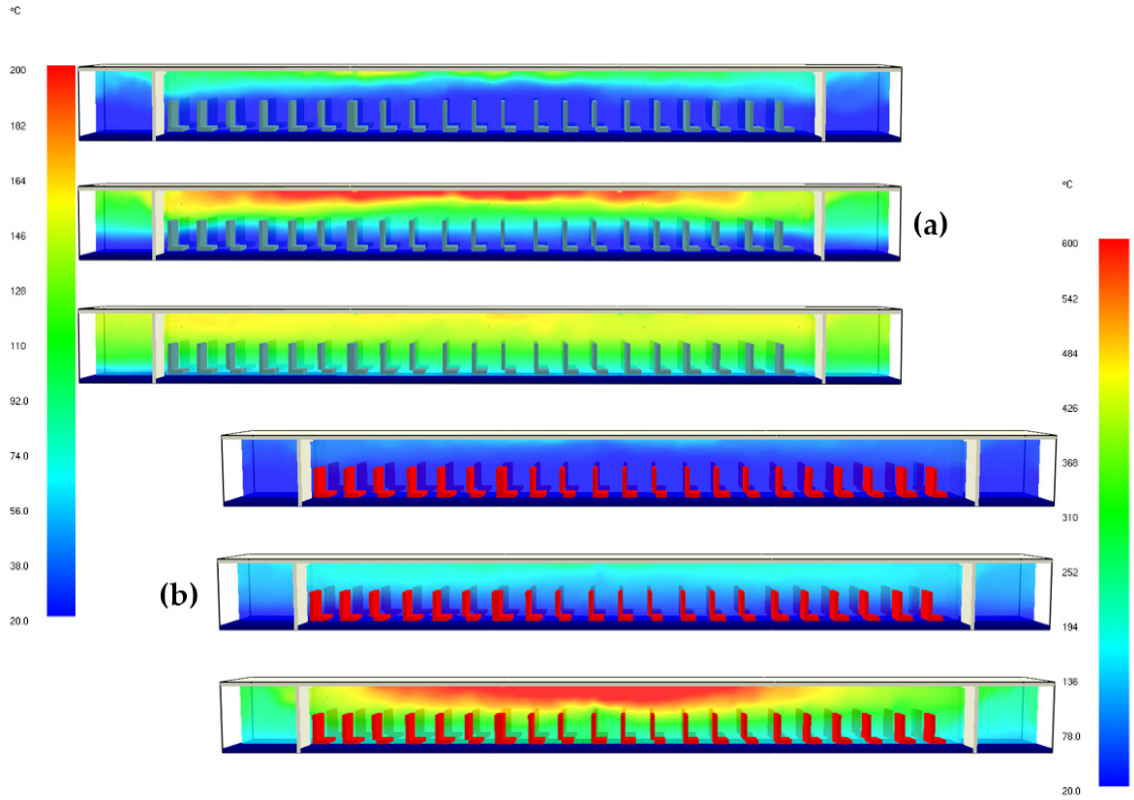

Figure 15. Temperature variations along the central plane of carriage after 40 s, 80 s and 120 s for (**a**) PN6 model and (**b**) PLY model.

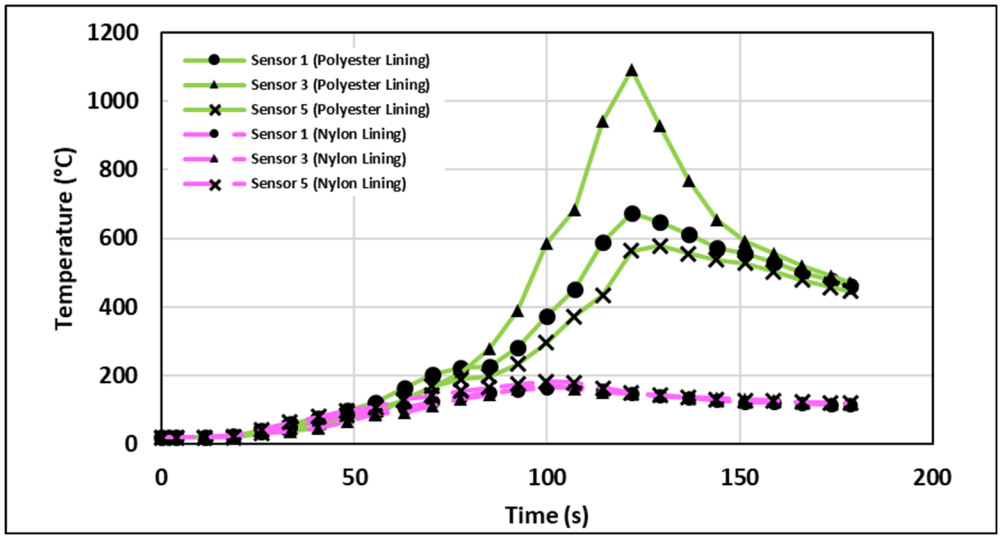

(**a**)

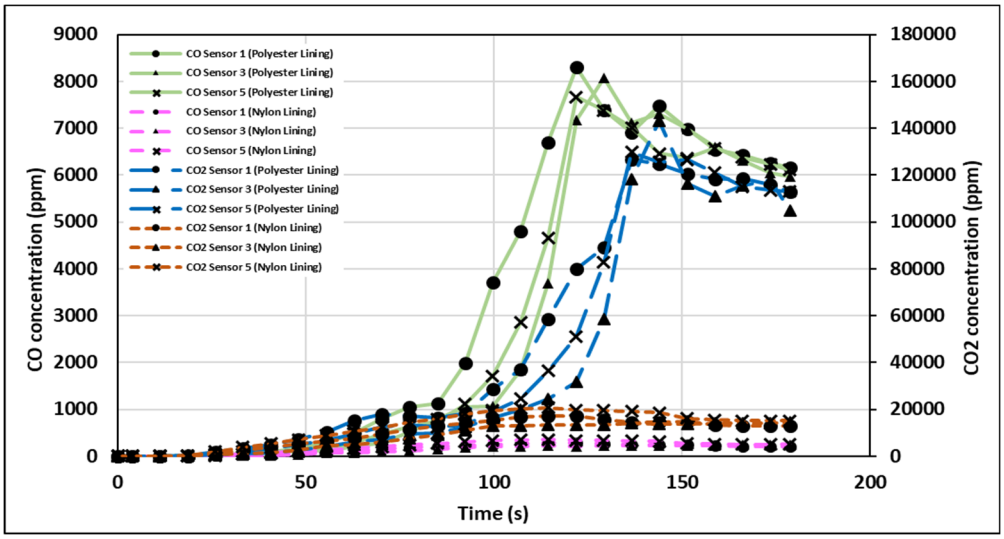

(**b**)

Figure 16. (**a**) Temperature comparison due to cabin upholstery. (**b**) Carbon gases concentrations for different upholstery materials.

The larger standard deviation of temperature within the PLY model implies that there was an increased difference in the flow regime. This caused larger eddies to occur within the polyester-type exhaust flow (due to the increased density and equivalent velocity), and thus caused a larger displacement of heat in each direction. This is in part validated by Figure 16a, which depicts that the difference in standard deviation between the three sensors for the PLY model was far higher than for the PN6 model. Figure 16b depicts the concentrations of product carbon-based gases from the two seating materials considered in the present study. It can be seen that the PLY material led to significantly higher concentrations of both CO and CO_2 100 s after ignition. Average readings of CO and CO_2 across the carriage, with the polyester-type material after 120 s, were around 7500 ppm and 60,000 ppm, respectively, which is 27× and 3.3× greater than those of the PN6 material. Given both the nature and magnitude of the levels of carbon monoxide exhaust gases produced by this lining, it can immediately be concluded that the polyester-type material is unsuitable for use from fire dynamics point of view. Further analysis of the growth rate of both carbon-based concentrations shows that within the initial 100 s, both material linings produced similar gas concentrations, validating that the material does not affect the smoke propagation, but rather contributes to the toxicity of smoke.

5. Conclusions

Due to the increasing number of passengers in the railway industry, greater understanding is required in the areas of fire dynamics and smoke toxicity in order to mitigate their life-threatening effects on humans, thus improving the safety of railway transport. The present study conducted extensive numerical investigations so as to understand these aspects. The results obtained show that the ignition position of fire affects local CO and CO_2 concentrations. Due to the difference in density between hot and cold gases within the railway carriage, thermal buoyancy forces the smoke generated to rise in the carriage. As more smoke is generated, it is propagated along the length of the carriage towards the areas of low concentration, until the whole carriage is filled with smoke. This indicated that initially, passengers relatively close to the fire area will experience the same smoke concentration as someone further away. The ignition position therefore significantly affects smoke layer height at each time interval, which has been depicted through the quantitative differences in smoke density. The ignition energy has been found to contribute to recorded smoke density levels, with a decrease of 50% in ignition energy corresponding to a 16% average reduction in smoke density. Changing the material lining of the seat has been found to significantly affect the carbon-product gas concentrations, with the polyester-type material producing 27×more CO and three times more CO_2

than the nylon-type counterpart, despite the relative insignificance of the mass of the material. This confirms the material's unsuitability for this application. The results obtained in this study can help in developing practical guidelines and standard operating procedures for passenger evacuation in the case of a fire in railway carriages and enclosed spaces. Further studies can be carried out in order to further understand fire dynamics, such as the effect of smoke accumulation on visibility within the carriage, fire forensics to help investigate fire incidents, etc. Furthermore, critical analysis of the effects of air conditioning on plume structure could be carried out perpendicular to the AC units.

Author Contributions: Conceptualization, M.C. and T.A.; methodology, M.C.; software, M.C.; validation, M.C. and T.A.; formal analysis, M.C. and T.A.; investigation, M.C.; resources, M.C.; data curation, M.C. and T.A.; writing—Original draft preparation, M.C.; writing—Review and editing, M.C. and T.A.; supervision, T.A.; project administration, T.A. All authors have read and agreed to the published version of the manuscript.

Funding: This research received no external funding.

Conflicts of Interest: The authors declare no conflict of interest.

Nomenclature

Latin Letters

A_{ign}	Ignition surface area (m^2)
$\bar{f}$	External force vector (excluding acceleration due to gravity) (N)
g	Acceleration due to gravity (m/s^2)
H	Height of domain (m)
H_c	Heat of combustion ($\frac{kJ}{kg}$)
j_m	Mass flux ($\frac{g}{m^2 \cdot s}$)
k_{sgs}	Sub-grid kinetic energy (J)
m	molar mass ($\frac{kg}{mol}$)
$\overline{\dot{m}_b'''}$	Mass production rate per unit volume of species by evaporating particles ($\frac{kg}{m^3 \cdot s}$)
$\bar{p}$	Filtered pressure vector (MPa)
$\overline{p}$	Pressure vector (MPa)
$\dot{q}_{ign}$	Ignition heat release rate (kW)
$\tilde{S}$	Solid component Favre filtered production rate
t	Time (s)
$\overline{\tilde{u}}$	Favre filtered velocity vector ($\frac{m}{s}$)
u	Small-scale function
$\tilde{u}$	Favre filtered velocity operator ($\frac{m}{s}$)
X_H	Fraction of hydrogen atoms within the soot
Y_s	Soot yield ($\frac{g}{g}$)

Greek Letters

β	Mass proportion of combustion ($\frac{kg}{kg}$)
δ	Kronecker delta
$\delta x \delta y \delta z$	Product of local mesh spacing in x, y and z directions (m^3)
Δ	Minimum eddy size
∇	$\bar{i}\frac{\partial}{\partial x} + \bar{j}\frac{\partial}{\partial y} + \bar{k}\frac{\partial}{\partial z}$
μ	Viscosity ($\frac{kg}{m \cdot s}$)
μ_t	Turbulent viscosity ($\frac{kg}{m \cdot s}$)
ν	Stochiometric coefficient
$\overline{\rho}$	Density vector ($\frac{kg}{m^3}$)
τ^{dev}	Total deviatoric stress (Pa)
τ^{sgs}	Sub-grid scale stress tensor (Pa)
$\overline{\emptyset}$	Favre filtered porosity

Subscripts

b	Bulk phase property

C	Carbon
CO	Carbon monoxide
d	Drag
F	Fuel
ijk	Gas phase cell indices
N	Nitrogen
s	Soot

References

1. Office of Rail and Road. *Passenger Rail Usage 2019-20—Q4 Statistical Release*; Office of Rail and Road: London, UK, 2020.
2. Electrified Rail Network: The Venefits. Available online: https://www.telegraph.co.uk/news/uknews/road-and-rail-transport/5892821/Electrified-rail-network-the-benefits.html (accessed on 10 September 2020).
3. European Commission. *Report on the Electrification of the Transport System*; European Commission: Brussels, Belgium, 2017.
4. Specific CO2 Emissions per Passenger-km and per Mode of Transport in Europe. Available online: https://www.eea.europa.eu/data-and-maps/daviz/specific-co2-emissions-per-passenger-3#tab-chart_1 (accessed on 17 June 2020).
5. Zhou, Y.; Wang, H.; Bi, H.; Gou, Q. Heat Release Rate of High-Speed Train Fire in Railway Tunnels. *Tunn. Undergr. Space Technol.* **2020**, *105*, 103563.
6. Li, Y.Z.; Inagson, H.; Lönnermark, A. Fire Development in Different Scales of Train Carriage. *Fire Saf. Sci.* **2014**, *11*, 302–315.
7. Li, Y.Z.; Inagson, H. A New Methodology of Design Fires for Train Carriages Based on Exponential Curve Method. *Fire Technol.* **2015**, *52*, 1449–1464.
8. Lee, D.H.; Park, W.H.; Hwang, J.; Hadjisophocleous, G. Full-Scale Fire Test of an Intercity Train Car. *Fire Technol.* **2016**, *52*, 1559–1574.
9. Arsonist Sets Fire in South Korean Subway. Available online: https://www.history.com/this-day-in-history/arsonist-sets-fire-in-south-korean-subway (accessed on 19 September 2019).
10. NTSB—National Transportation Safety Board. *Aircraft Accident Report: Air Canada flight 797, 1986*; NTSB—National Transportation Safety Board, US Government: Washington, DC, USA.
11. Fire Safety on Trains. Available online: https://www.railengineer.co.uk/2016/12/22/fire-safety-on-trains/ (accessed on 19 September 2019).
12. EN 45545-2 European Railway Standard for Fire Safety. Available online: https://dge-europe.com/en-45545-european-railway-standard-fire-safety/ (accessed on 15 September 2020).
13. Hjohlman, M.; Försth, M.; Axelsson, J. *Design Fire for a Train Compartment*; Technical Research Institute of Sweden: Borås, Sweden, 2009; ISBN 978-9-1858-2979-8.
14. Li, S.C.; Huang, D.F.; Meng, N.; Chen, L.F.; Hu, L.H. Smoke Spread along a Corridor Induced by an Adjacent Compartment Fire with Outdoor Wind. *Appl. Therm. Eng.* **2017**, *111*, 420–430.
15. Jia, F.; Galea, E.R.; Patel, M.K. The Prediction of Fire Propagation in Enclosure Fires. *Fire Saf. Sci.* **1997**, *5*, 439–450.
16. Galea, E.R.; Wang, Z.; Jia, F. Numerical Investigation of the Fatal 1985 Manchester Airport B737 Fire. *Aeronaut. J.* **2017**, *121*, 287–319.
17. Stollard, P. *Fire from First Principles a Design Guide to International Building Fire Safety*, 4th ed.; Roultedge: London, UK, 2014; ISBN 9781317919049.
18. Tsukahara, M.; Koshiba, Y.; Ohtani, H. Effectiveness of Downward Evacuation in a Large-scale Subway Fire using Fire Dynamics Simulator. *Tunn. Undergr. Space Technol.* **2011**, *26*, 573–581.
19. Enbaya, A.A.F.; Asim, T.; Mishra, R.; Raj Rao, B.K.N. Numerical Analysis of a Railway Compartment Fire using Computational Fluid Dynamics. *Int. J. COMADEM* **2015**, *18*, 37–44.
20. Jung, J.T.; Kang, S.G.; Yoon, H.J.; Shin, K.B.; Lee, J.K.; Stochino, F. Analysis of Heat and Smoke Flow according to Platform Screen Door and Fan Conditions on Fire in Underground Platform. *Adv. Civ. Eng.* **2018**, *2018*, 1–8.
21. Chow, W.K.; Lam, K.C.; Fong, N.K.; Li, S.S.; Gao, Y.; Yeoh, G. Numerical Simulations for a Typical Train Fire in China. *Model. Simul. Eng.* **2011**, *2011*, 1–7.
22. Drysdale, D. *An Introduction to Fire Dynamics*; 2nd ed.; Wiley: Chichester, UK, 2004; ISBN 047-1-972-916.

23. Wang, F.; Wang, M.; Carvel, R.; Wang, Y. Numerical Study on Fire Smoke Movement and Control in Curved Road Runnels. *Tunn. Undergr. Space Technol.* **2017**, *6*, 1–7.
24. Ozetkin, E.S. Heat and Mass Transfer due to a Small Fire in an Aircraft Cargo Compartment. *Int. J. Heat Mass Transf.* **2014**, *73*, 562–573.
25. Stec, A.A. Fire Toxicity—The Elephant in the Room? *Fire Saf. J.* **2017**, *91*, 79–90.
26. Stec, A.A.; Hull, T.R.; Purser, D.A.; Purser, J.A. Fire Toxicity Assessment: Comparison of Asphyxiant Yields from Laboratory and Large Scale Flaming Fires. *Fire Saf. Sci.* **2014**, *11*, 404–418.
27. Alarie, Y. Toxicity of Fire Smoke. *Crit. Rev. Toxicol.* **2002**, *32*, 264–282.
28. Carbon Monoxide Questions and Answers. Available online: https://www.cpsc.gov/Safety-Education/Safety-Education-Centers/Carbon-Monoxide-Information-Center/Carbon-Monoxide-Questions-and-Answers (accessed on 13 January 2020).
29. Henderson, R.E. *Carbon Dioxide Measures Up As A Real Hazard*; BW Technologies by Honywell: Calgary, AB, Canada, 2006.
30. Mouritz, A.P.; Gibson, A.G. *Fire Properties of Polymer Composite Materials;* Springer: Dordrecht, The Netherlands, 2006; ISBN 978-1-4020-5356-6.
31. Deans, T.; Schiraldi, D.A. Flammability of Polyesters. *Polymer* **2014**, *55*, 825–830.
32. Global Market Study on Train Seat Materials. Available online: https://www.persistencemarketresearch.com/market-research/train-seat-materials-market.asp (accessed on 1 June 2020).
33. McKenna, S.T.; Birtles, R.; Dickens, K.; Walker, R.G.; Spearpoint, M.J.; Stec, A.A.; Hull, T.R. Flame Retardants in UK Furniture Increase Smoke Toxicity More Than They Reduce Fire Growth Rate. *Chemosphere* **2018**, *196*, 429–439.
34. Cai, W. Mussel-inspired Functionalization of Electrochemically Exfoliated Graphene: Based on self-polymerization of dopamine and its suppression effect on the fire hazards and smoke toxicity of thermoplastic polyurethane. *J. Hazadr. Mater.* **2018**, *352*, 57–69.
35. Siemans Viaggio Comfort Push/Pull Train. Available online: https://www.railway-technology.com/projects/siemens-viaggio-comfort-push-pull-train/ (accessed on 10 February 2020).
36. McGrattan, K.; McDermott, R.; Vanella, M.; Hostikka, S.; Floyd, J. *Fire Dynamics Simulator User's Guide*, 6th ed.; NIST—National Institute of Standards and Technology: Gaithersburg, MD, USA, 2020, doi:10.6028/NIST.SP.1019.
37. Rodriguez, S. *Applied Computational Fluid Dynamics and Turbulence Modelling*; Springer: Cham, Switzerland, 2019; ISBN 978-3-0302-8691-0.
38. Vreman, B.; Guerts, B.; Kuerten, H. Subgrid Modelling in LES of Compressible Flow. *Appl. Sci. Res.* **1995**, *54*, 191–203.
39. McGrattan, K.; McDermott, R.; Vanella, M.; Hostikka, S.; Floyd, J. *Fire Dynamics Simulator Technical Reference Guide*, 6th ed.; Mathematical Model; NIST—National Institute of Standards and Technology: Gaithersburg, MD, USA, 2020; Volume 1, doi:10.6028/NIST.SP.1018.
40. Polyamide or Nylon: Complete Guide. Available online: https://omnexus.specialchem.com/selection-guide/polyamide-pa-nylon (accessed on 28 November 2019).
41. Węgrzyński, W.; Vigne, G. Experimental and Numerical Evaluation of the Influence of the Soot Yield on the Visibility in Smoke in CFD Analysis. *Fire Saf. J.* **2017**, *91*, 389–398.
42. Hurley, M.J.; Gottuk, D.; Hall, J.R., Jr.; Harada, K.; Kuligowski, E.; Puchovsky, M.; Torero, J.; Watts, J.M., Jr.; Wieczorek, C. Inferring Functional Relationships from Conservation of Gene Order. In *SPFE Handbook of Fire Protection Engineering*, 5th ed.; Springer: New York, NY, USA, 2016; pp. 3467–3469. ISBN 978-1-4939-2565-0.
43. Updated FDS Combustion and Fuel Composition Calculators. Available online: https://www.thunderheadeng.com/2015/09/updated-fds-combustion-and-fuel-composition-calculators/ (accessed on 9 September 2020).
44. *ISO 7730:2005—Ergonomics of the Thermal Environment*; International Organization of Standardization: Geneva, Switzerland, 2005.

45. Hong, W.H. *The Process and Controlling Situation of Daegu Subway Fire Disaster*; Urban Environmental System & Research Lab: Daegu, Korea, 2004.
46. Both, K.; Haack, A. *Present-Day Design Fire Scenarios and Comparison with Test Results and Real Fires*; First International Symposium: Prague, Czechia, 2004.